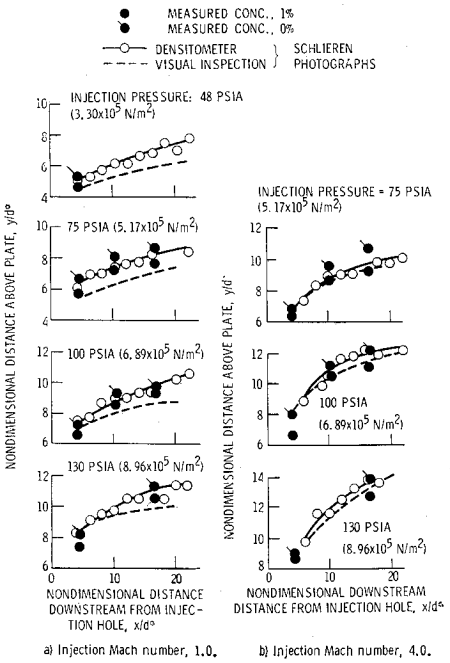

Fig. 3 Helium jet boundary, comparison of measurement techniques.

Centerplane concentration measurements obtained with a mass spectrometer were made at 4, 10, and 17 injection throat diameters downstream of the injection point. Details of the concentration measurement technique are given in Ref. 2.

Schlieren photographs of 0.1 sec exposure were made with a conventional single pass system with the knife edge oriented perpendicular to the freestream flow. The photographs were analyzed with a double beam recording microdensitometer. The densitometer beam scanned the photographs in a direction normal to the flat plate 4 to 20 injection throat diameters downstream of the injection point. The distance from the surface of the flat plate to the point where the photographic density decayed to the background level was considered to be the jet penetration, or boundary location, at each downstream position. The apparent outer edge of the jet, that appeared as a longitudinal streak, was also measured by visual inspection of the photographs.

Results and Discussion

Typical results of jet penetration obtained from densitometer measurements, visual inspection of the schlieren photographs, and concentration measurements are shown in Fig. 3. The penetration distance normal to the flat plate y and the downstream distance from the injection orifice x are nondimensionalized by the injection throat diameter, d^*. The solid points represent volumetric helium concentrations of 0 and 1% on the centerplane.

In most instances the jet boundary obtained by densitometer analysis of the schlieren photographs was found to lie within the region bounded by the 0 and 1% concentration points. It thus appears, that if the jet can be visualized by the schlieren method, penetration can be quite accurately measured by the technique described in this Note. The visually located boundary, indicated as the "jet boundary" in Fig. 1, in some cases corresponded to the region bounded by the 0 and 1% concentration points. However, use of the visually located boundary underestimated penetration by as much as 15%. Visual measurements might however be acceptable for rapid qualitative estimates of penetration. Independent measurements of the jet boundary location from the schlieren negatives by two observers were identical. It was also established that effects of photographic emulsion type, exposure time, and schlieren sensitivity settings had little effect on the accuracy of the jet boundary measurements. This was established by making measurements using Panatomic and Tri-X film types, varying the exposure time from 0.01 to 0.005 sec, and varying the adjustment of the knife edge.

Zukoski and Spaid,[4] observed what they considered to be a jet streamline with nitrogen and argon injection. They could not however observe this feature with helium injection. This feature was most likely, as suggested by Schetz, Hawkins, and Lehman,[6] a portion of the jet shock structure. In the present study it was also noted that jet shock structure could be observed with nitrogen and argon but not with helium injection. On the other hand, the streak indicating the injectant path, as shown on Fig. 1 was observed only for helium. Thus, the technique described here, may be useful only for helium injection. However, the technique described in this Note may provide a valuable alternate method of measuring jet penetration for gases such as helium, where the injectant path rather than the shock structure can be visualized.

References

[1] Torrence, M. G., "Concentration Measurements of an Injected Gas in a Supersonic Stream," TN D-3860, 1967, NASA.

[2] Povinelli, L. A., Povinelli, F. P., and Hersch, M., "A Study of Helium Penetration and Spreading in a Mach 2 Airstream Using a Delta Wing Injector," TN D-5322, 1969, NASA.

[3] Povinelli, F. P., Povinelli, L. A., and Hersch, M., "Effect of Angle of Attack and Injection Pressure on Jet Penetration and Spreading from a Delta Wing in Supersonic Flow," TM X-1889, 1969, NASA.

[4] Zukoski, E. E. and Spaid, F. W., "Secondary Injection of Gases into a Supersonic Flow," *AIAA Journal*, Vol. 2, No. 10, Oct. 1964, pp. 1689–1696.

[5] Vranos, A. and Nolan, J. J., "Supersonic Mixing of a Light Gas and Air," *AIAA Propulsion Joint Specialists Conference*, New York, 1965.

[6] Schetz, J. A., Hawkins, P. F., and Lehman, H., "Structure of Highly Underexpanded Transverse Jets in a Supersonic Stream," *AIAA Journal*, Vol. 5, No. 5, May 1967, pp. 882–884.

Laser Velocimeter Used to Find Transition Region

B. G. McKinney*
Marshall Space Flight Center, Huntsville, Ala.
AND
A. R. Shouman†
New Mexico State University, Las Crusas, N. Mex.

OSBORNE Reynolds[1] is credited with finding the unifying principle for explaining the phenomena of the transition of flow from the laminar regime to the turbulent regime first observed and investigated by Hagen.[2,3] Reynolds measured the pressure drop through a known length of pipe, used the average velocity $\bar{V}$ to calculate $D\bar{V}\rho/\mu$ (the Reynolds number, Re), and determined the critical Reynolds number (Re_{crit}) for transition as the value at which the friction coefficient calculated from the pressure drop took a compara-

Received January 16, 1970; revision received February 18, 1970.

* Technical Assistant, Life Support and Environmental Branch, Astronautics Laboratory, Science and Engineering Directorate.

† Professor, Department of Mechanical Engineering.

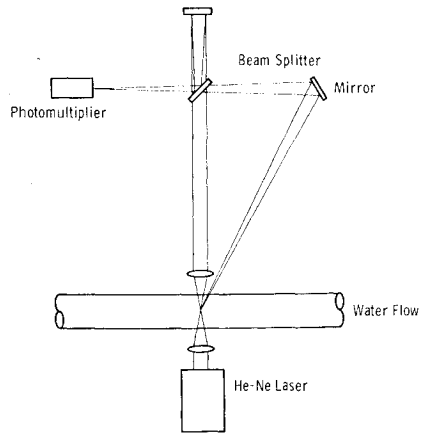

Fig. 1 Optical setup.

tively sudden increase. (Here D, ρ, and μ are the tube's inside diameter, the fluids density, and viscosity, respectively.) Recent investigations examined the nature of transition in more detail. Rotta[4] recorded V as a function of time at different radial locations in a pipe and demonstrated the fluctuation of flow between laminar and turbulent flow. Very recently, Foreman, Lewis, George et al.[5,6] described the technique for using the laser beam to determine velocities in fluids through measurement of the Doppler effect. The same technique is used in this investigation. The advantages of the laser velocimeter are: 1) the possibility of exploring the flow velocity field with no disturbance to the field; and 2) the very fast response of the velocimeter to the flow conditions. In this investigation the laser velocimeter is used to determine the inception of the transition region at the centerlines of glass tubes. The centerline frequencies, from which velocities may be obtained, were measured, and from the flow rates recorded by the flow meter, Re_{crit} was determined for each tube.

Description of Equipment

The optical setup around the water flow tube is sketched in Fig. 1. A flow loop provides a constant water flow rate from a constant-head tank (with an overflow recirculating line) through the glass tube and flow meter. Glass tubes of 0.400-, 0.865-, 1.040-, 1.375-, and 1.875-in. inside diameters have been used. A He-Ne gas laser provides a beam of coherent light that was directed through the glass tube. The focal point is located at the center of the tube. Light is scattered from the focal point by small particles in the water. A lens is arranged at a known angle to receive the light scattered at that angle. The light differs in frequency from the parent beam because of the Doppler effect produced by the motion of small plastic spheres in the liquid. These two light beams, when recombined on the cathode of a photomultiplier, produce a heterodyne signal, the frequency of which is directly proportional to the longitudinal component of the fluid velocity at the focal point. This signal also exhibits amplitude variations, that depend on the size and locations of the particles in the scattering volume. It is amplified and band-limit filtered to remove undesirable noise. The resulting signal is fed into a commercial (Wavetek) phase-lock loop, whose output is recorded on an oscillograph.

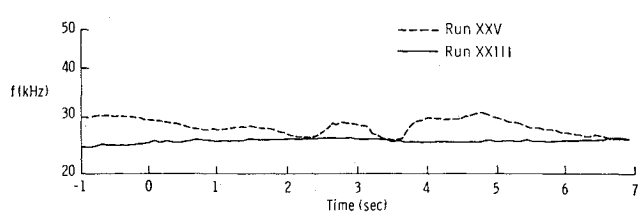

Fig. 2 Frequency vs time.

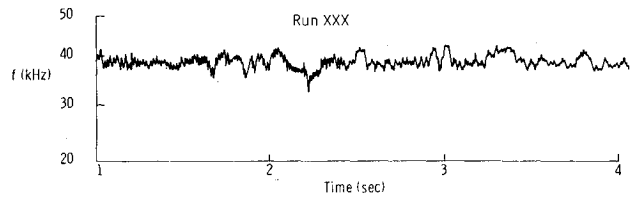

Fig. 3 Frequency vs time.

Results and Discussion

Figure 2 shows frequency vs time for examples of data where flow is completely laminar (run XXIII) and where transition is beginning in a 1.87-in. diam tube. Figure 3 presents data for a case with completely turbulent flow. Figure 4 shows Re_{crit} vs D.

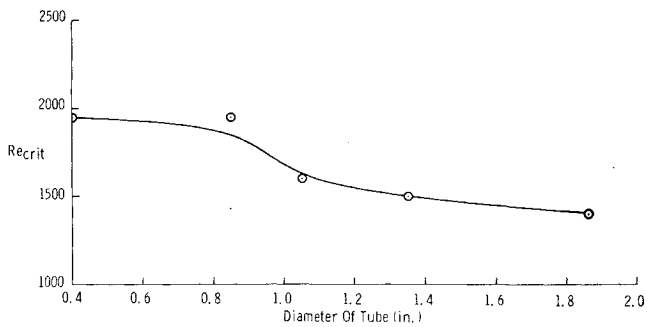

Fig. 4 Reynolds number vs diameter of tube at first transition.

For fully developed laminar flow, $\bar{V}$ should equal one-half the centerline velocity $\bar{V}_{cl}$. Table 1 compares 0.5 $\bar{V}_{cl}$ to the $\bar{V}$ determined from flow rate. The largest error shown by the data is $\approx 6\%$.

To ensure that fully developed flow was present at the section where the measurement was taken, a reading was

Table 1 Comparison of velocities

f, kHz	V_{cl} calculated from f, fps	$0.5V_{cl}$, fps	$\bar{V}$ from flow rate, fps
200	0.98	0.49	0.481
95	0.47	0.235	0.236
55	0.27	0.135	0.135
48	0.24	0.12	0.112
25	0.13	0.065	0.066

taken with the laser velocimeter at a smaller flow rate than that at which the first indications of transition occurred. This reading was checked by comparing it with the $\bar{V}$ calculated from the measured flow rate. Through this procedure it was established that the flow just preceding transition was fully developed and laminar. In all cases, the station at which the velocity was measured was 50 diam or more from the tube entrance.

From the data obtained it appears that Re_{crit} decreases when tube diameter is increased within the range of diameters examined. The values of Re_{crit} measured in this investigation are smaller than those previously reported by others. The magnitude of Re_{crit} should have no effect on the trend of the data shown by this investigation.

References

[1] Reynolds, O., "An Experimental Investigation of the Circumstances Which Determine Whether the Motion of Water Will be Direct or Sinuous, and of the Law of Resistance in Parallel Channels," *Philosophical Transactions of the Royal*

Society of London, Vol. 174, Pt. III, 1883, pp. 935–982; also *Scientific Papers*, Vol. 2, pp. 51–105.

[2] Hagen, G., "On the Motion of Water in Narrow Cylindrical Tubes," *Annalen der Physik*, Vol. 46, 1839, pp. 423–442.

[3] Hagen, G., "On the Influence of Temperature on the Movement of Water Through Pipes," *Abhandlungen der Deutschen Akademie der Wissenschaften*, Berlin, 1854, pp. 17–35.

[4] Rotta, J., "Experimenteller Beitrag zur Entstehung Turbulenter Strömung im Rohr," *Ingenieur-Archiv*, Vol. 24, No. 4, 1956, pp. 258–281.

[5] Foreman, J., Lewis, R. and George, E., "Measurement of Localized Flow Velocities in Gases with a Laser Flow Meter," *Applied Physics Letters*, Vol. 7, No. 4, Aug. 1966, pp. 77–78.

[6] Foreman, J. et al., "Fluid Flow Measurement with a Laser Doppler Velocimeter," *IEEE Journal of Quantum Electronics*, Vol. QE-2, No. 8, Aug. 1966, pp. 260–266.

Impact Point Dispersion due to Spin Reversal

ALI HASAN NAYFEH*
Aerotherm Corporation, Mountain View, Calif.
AND
GERALD G. WILSON†
Sandia Corporation, Albuquerque, N. Mex.

Introduction

IT has been recognized that small re-entry vehicles can experience uncontrolled anomalous roll motions during reentry. The principal deleterious effect of these motions is the occurrence of a roll resonance or spin-through-zero roll-rate condition with attendant unacceptably large lateral loads and/or large impact point dispersions. To eliminate the possibility of encountering roll resonance, control of the roll rate to subresonant rates has been suggested. However, some candidate control schemes do not avoid the possibility of experiencing spin rate reversal. The purpose of this Note is to assess analytically the magnitudes of the resulting dispersions and their sensitivity to the variation of trajectory and body parameters. Also, the differences between the present analysis and the more restrictive previous work by Fuess[1] and Crenshaw and Tessitore[2] are indicated.

Analysis

For small roll rates, and away from resonance, the trim angle of attack in a body fixed coordinate system can be approximated by the complex number

$$\delta = \beta_t + i\alpha_t \tag{1}$$

where α_t and β_t are the components of the static trim angle of attack. Moreover, the variation of the roll rate, p, with time is given by

$$dp/dt = (qAd/I_x)C_l \tag{2}$$

where q is the dynamic pressure, A is the body cross-sectional area, d is the body diameter, I_x is the axial moment of inertia, and C_l is the roll moment coefficient and is given by[3]

$$C_l = \frac{c\alpha_t}{d} - \frac{c}{d}\Delta C_{N0}\cos\lambda + C_{lf}\frac{pd}{2V} + C_{l\theta}\,\theta + C_{lp}\frac{pd}{2V} \tag{3}$$

The first term on the right-hand side of Eq. (3) is due to the combination of a center of gravity (c.g.) offset and a trim δ. Without loss of generality, the c.g. offset plane is taken orthogonal to the plane of the α_t component of the trim δ. The second term is caused by a normal force component, ΔC_{N0}, which together with its orientation, λ, are independent of δ. This normal force is caused by the geometric nose asymmetries. The third term represents the roll damping due to friction, while the fifth term represents the roll damping due to grooves in the body surface. The fourth term represents the ablation-grooving roll driving moment.

If the dispersion due to roll reversal is denoted by the complex number $z = z_\beta + iz_\alpha$, then

$$m\frac{d^2z}{dt^2} = Le^{iP}, \qquad P = \int_0^t p(\tau)d\tau \tag{4}$$

where m is the body mass, P is the roll orientation, and L is the lift force and approximately given by

$$L = qA\delta(C_{N\alpha} - C_A) \tag{5}$$

where $C_{N\alpha}$ is the normal force derivative per radian and C_A is the axial force coefficient. Integrating once Eq. (4), and separating real and imaginary parts lead to

$$\dot{z}_\beta = \int_0^t \frac{L}{m}(\beta_t\cos P - \alpha_t\sin P)dt \tag{6}$$

$$\dot{z}_\alpha = \int_0^t \frac{L}{m}(\beta_t\sin P + \alpha_t\cos P)dt \tag{7}$$

For large roll rates, the integrals in Eqs. (6) and (7) average out, and hence most of the contribution comes from the neighborhood of small roll rates, especially near zero roll rate if it exists. Thus, L and C_l can be taken to be constants, and equal to their values at the time of roll through zero, t_z. In order to estimate the integrals in Eqs. (6) and (7), we let

$$\pi s^2 = (qAd/I_x)C_l(t - t_z)^2 \tag{8}$$

Then,

$$\dot{z}_\beta = \chi[(\beta_t\cos P_z - \alpha_t\sin P_z)I_1 - (\beta_t\sin P_z + \alpha_t\cos P_z)I_2] \tag{9}$$

$$\dot{z}_\alpha = \chi[(\alpha_t\cos P_z + \beta_t\sin P_z)I_1 - (\alpha_t\sin P_z - \beta_t\cos P_z)I_2] \tag{10}$$

where

$$P_z = \int_0^{t_z} p(t)dt$$

$$\chi = (C_N\dot{z} - C_A)/m[\pi I_x Aq/dC_l]^{1/2} \tag{11}$$

$$I_1 = \int_{-\infty}^{\infty}\cos\frac{\pi}{2}s^2ds \qquad \text{and} \qquad I_2 = \int_{-\infty}^{\infty}\sin\frac{\pi}{2}s^2ds \tag{12}$$

The limits of integration for I_1 and I_2 are set $+\infty$ and $-\infty$ because the contribution from the large values of s is small. The integrals I_1 and I_2 are the Fresnel integrals, and each has the value of unity.

The velocity perturbation $|\dot{z}|$ normal to the body velocity is then given by

$$|\dot{z}| = (\dot{z}_\alpha^2 + \dot{z}_\beta^2)^{1/2} = \chi[2(\beta_t^2 + \alpha_t^2)]^{1/2} \tag{13}$$

The perturbation in flight path angle γ_z due to roll reversal is then

$$\gamma_z = |\dot{z}|/V \tag{14}$$

Hence the semiminor axis, b_z, and the semimajor axis, a_z, of

Received January 16, 1970; revision received March 27, 1970. This work was supported by U.S. Atomic Energy Commission under contract to Sandia Laboratories and Sandia contract to Aerotherm Corporation.

* Manager, Mathematical Physics Department. Member AIAA.

† Staff Member, Aeroballistics Division.